THE AMERICAN SOCIETY OF MECHANICAL ENGINEERS
345 E. 47 St., New York, N.Y. 10017

Convective Transport Phenomena on the Suction Surface of a Turbine Blade Including the Influence of Secondary Flows Near the Endwall

P. H. CHEN*
R. J. GOLDSTEIN
Department of Mechanical Engineering
University of Minnesota
Minneapolis, Minnesota, 55455

ABSTRACT

A naphthalene sublimation technique is employed to study the mass transfer distribution on the suction (convex) surface of a simulated turbine blade. Comparison with a heat transfer study shows good agreement in the general trends in the region of two-dimensional flow on the blade.

Near the endwall, local convective coefficients on the suction surface are obtained at 4608 locations from two separate runs. The secondary flows in the passage significantly affect the mass transfer rate on the suction surface and their influence extends to a height of 75% of the chord length, from the endwall, in the trailing edge region. The mass transfer rate in the region near the endwall is extremely high due to small but intense vortices. Thus, a large variation in the mass transfer distribution occurs on the suction surface, from a mass transfer Stanton number of 0.0005 to a maximum of 0.01. In the two-dimensional flow region, the mass transfer distributions at two different Reynolds number are presented.

NOMENCLATURE

AC	axial chord length, see Figure 2; AC = 145.3 mm in the present study
C	chord length of the test blade, see Figure 2; C = 169.1 mm in the present study
c_p	specific heat, J/(kg K)
C_{ps}	static pressure coefficient, $(P_s - P_{1s})/(0.5\rho U_1^2)$
C_1	an empirical constant, (Eqs. 7 and 8)
d	diameter of the cylinder or the leading edge of the test blade, d=18.3 mm in the present study
d_w	diameter of the trip wire, 1.59 mm and 3.76 mm for the case of the thin and the thick inlet boundary layer, respectively
D	diffusion coefficient of naphthalene in air, m^2/s, D=0.076 m^2/s at 298.15 K and 0.1013MPa
h	local heat transfer coefficient
h_m	local mass transfer coefficient, (Eq.1), m/s
H	shape factor of the approaching endwall boundary layer, δ_1/δ_2, measured 145 mm upstream of the leading edge of the test blade
k	thermal conductivity of air
L_{sb}	change in local naphthalene sublimation thickness during exposure in an air stream in, m
$\dot{m}$	local naphthalene mass transfer rate per unit area, $kg/(m^2s)$
n	exponent in empirical correlations (Eqs. 7 and 8)
Nu	Nusselt number, hC/k
Nu_d	Nusselt number, hd/k
p	exponent in empirical correlations (Eqs. 7 and 8)
P	total pressure
P_s	static pressure measured on the blade surface
P_{1s}	static pressure upstream of the cascade
$P_{v,w}$	local naphthalene vapor pressure at the test blade surface, N/m^2
Pr	Prandtl number, $\mu c_p/k$
R_{Vsc1}	reattachment line of the suction side corner vortex 1(V_{sc1}), shown in Figure 8
R_{Vsc2}	reattachment line of the suction side corner vortex 2(V_{sc2}), shown in Figure 8

*Presently at National Taiwan University, Department of Mechanical Engineering Taipei, Taiwan, ROC.

Presented at the International Gas Turbine and Aeroengine Congress and Exposition
Orlando, FL June 3-6, 1991
This paper has been accepted for publication in the Transactions of the ASME
Discussion of it will be accepted at ASME Headquarters until September 30, 1991

R_{Vsh}/R_{Vp}	reattachment line of the passage vortex and the suction side horseshoe vortex, shown in Figure 8
R_{2D}	reattachment line of the two-dimensional separation bubble on the suction surface of a turbine blade, shown in Figure 8
q	heat flux
Re_d	Reynolds number, $U_1 d/\upsilon$ in the present study and $U_\infty d/\upsilon$ in earlier studies of a cylinder in a cross-stream
Re	Reynolds number
Re_1	inlet Reynolds number, $U_1 C/\upsilon$
Re_2	exit Reynolds number, $U_2 C/\upsilon$
S_p	pressure (concave) side curvilinear distance from the stagnation line of the test blade, shown in Figure 2, - Note that the stagnation line is determined from flow visualization results in the present study and $S_p/C = 1.06$ at the trailing edge
S_s	suction side curvilinear distance from the stagnation line of the test blade, shown in Figure 2, - Note that the stagnation line is determined from flow visualization results in the present study and $S_s/C = 1.355$ at the trailing edge
S_{Vp}	separation line of the passage vortex, shown in Figure 8
S_{Vsc1}	separation line of the suction side corner vortex 1(V_{sc1}), shown in Figure 8
S_{Vsc2}	separation line of the suction side corner vortex 2(V_{sc2}), shown in Figure 8
S_{Vsh}	separation line of the suction side horseshoe vortex, shown in Figure 8
S_1-S_2	separation line of the horseshoe vortex on the wall, shown in Figure 7
S_{2D}	two-dimensional laminar separation line on the suction surface, shown in Figure 8
Sc	Schmidt number, υ/D, ≈ 2.04 for naphthalene at 298.15K and 0.1013Mpa
Sh	Sherwood number, $h_m C/D$
St	heat transfer Stanton number, $h/\rho C_p U_1$
St_m	local mass transfer Stanton number, h_m/U_1
$\overline{St_m}$	average mass transfer Stanton number over the whole curvilinear distance on the suction side, (S_S)
T	absolute temperature, K
T_w	temperature of wall, K
T_∞	temperature of free-stream, measured 145mm upstream of the leading edge of the test blade, K
Tu	turbulence intensity in approaching free-stream
U	free-stream velocity in the blade passage
U_1	velocity upstream of the cascade, see Table 3
U_2	velocity measured at the midspan of the exit of the cascade, see Table 3, m/s
U_∞	approach free-stream velocity for the study of a cylinder in a cross stream, m/s
V_p	passage vortex, shown in Figure 7
V_{pc}	pressure side corner vortex, shown in Figure 7
V_{ph}	pressure side horseshoe vortex, shown in Figure 7
V_{pLc}	pressure side leading edge corner vortex, shown in Figure 7
V_{sc1}	suction side corner vortex 1, shown in Figure 7
V_{sc2}	suction side corner vortex 2, shown in Figure 7
V_{sh}	suction side horseshoe vortex, shown in Figure 7
V_{sLc}	suction side leading edge corner vortex, shown in Figure 7
X	distance from the center of the rotary table on the horizontal plane and normal to the central line of the LVDT, cm, shown in Figure 3
X_n	normalized dimension of the blade, shown in Figure 2
Y	distance from the center of the rotary table on the horizontal plane and parallel to the central line of the LVDT, shown in Figure 3
Y_n	normalized dimension of the blade, shown in Figure 2
Z	vertical distance from the top wall of the test section
Z_r	direction along the central line of the rotating table, shown in Figure 3
α	inlet flow angle of the cascade, degree, shown in Figure 2
δ_1	displacement thickness of the approaching endwall boundary layer, measured 145mm upstream of the leading edge of the test blade
δ_2	momentum thickness of the approaching endwall boundary layer, measured 145mm upstream of the leading edge of the test blade
Δt	total time the test blade is exposed in the air-stream, s
μ	dynamic viscosity of air
υ	kinematic viscosity of air
ρ_s	density of solid naphthalene, ρ_s=1145 kg/m^3 at 298.15K
$\rho_{v,w}$	local naphthalene vapor density on the test blade surface

$\rho_{v,\infty}$ naphthalene vapor density in the mainstream, zero in the present study

θ angular direction of the rotating table, shown in Figure 3

INTRODUCTION

In modern aircraft gas turbine engines, the turbine inlet temperature has been steadily increased to at least 1780K (Guenette et al., 1989). High temperatures and transient temperature response of engine components can produce large thermal stresses. The life of highly stressed components decreases significantly with increasing metal temperatures. Knowledge of the detailed heat transfer distribution is required to design such machines for thousands of hours of continuous operation without failure. In order to predict the service life of the engine, it is essential to have both local temperature levels of the hot gas and local temperature gradients from the hot gas to the components. After giving a brief summary of related studies, Graham (1979) and Dyban (1982) both listed several fundamental mechanisms that affected the heat transfer to gas turbine blades. These interrelated mechanisms include rotating effects, secondary flows, boundary layer transition, unsteady wakes, free-stream turbulence, surface curvature, injected coolant flow, flow separation, shock, etc.. Taylor (1980) also suggested further studies on the combined effects of these parameters and the need to investigate specific problems to justify or to improve numerical predictions. The present state of art in numerical predictions is generally not satisfactory for engine design due to difficulties in the prediction of boundary layer flows and heat transfer along a blade surface. More experimental work is needed to improve our understanding of the convective transport from the hot gas to turbine blades. The purpose of the present study is to obtain detailed mass transfer distributions on a (simulated) turbine blade under the influence of secondary flows. These measured mass (heat) transfer distributions can be used to validate and improve confidence in the accuracy of existing computational codes and through the heat/mass transfer analogy can be used to predict heat transfer to a blade.

For four decades, numerous studies have been conducted to investigate the external heat transfer processes from the hot gas to the blades. Smith (1948) reviewed early works conducted in the 1940's. The relation between the exit Reynolds number and the mean Nusselt number for five different blades was presented. He showed that the mean Nusselt number could change significantly for different blade profiles and increase with increasing exit Reynolds number for all blades. Wilson and Pope (1958) measured the local heat transfer along both surfaces of a heated blade over a wide range of inlet flow angle and exit Reynolds number. They presented many valuable observations. The transition from laminar to turbulent boundary layer flow can cause a steep rise on the heat transfer distribution on both surfaces. Higher mainstream turbulence as well as surface roughness result in a higher heat transfer rate.

More recently, turbine blade heat transfer has been investigated using several new methods such as a shell blade technique, a transient technique (or a short duration measurement technique conducted in a shock tunnel), a naphthalene sublimation technique, and a liquid crystal technique. By applying the shell blade or similar technique, Turner (1971), Dyban and Glushchenko (1975), York et al. (1979), Mukherjee (1979), Bayley and Priddy (1981), Turner et al. (1985), and Priddy and Bayley (1985) reported blade heat transfer results. Bayley et al. (1981) showed the effect of free-stream turbulence intensity in the range of 0.5 to 32 % and frequency of free-stream perturbation on the heat transfer rate to turbine blades. The heat transfer rate along both surfaces is slightly raised as the frequency of free-stream perturbation increased from 5KHz to 10 KHz. On the suction (convex) surface, the laminar to turbulent transition was suppressed at Tu $\approx$ 17%. The effect of surface roughness on the blade heat transfer rate was examined by Turner et al. (1985). Early transition and a fairly uniform increase of heat transfer are caused by the surface roughness. A discussion on the natural transition on both surfaces of several different blades was presented by Priddy et al. (1985). They concluded that the natural transition on the suction surface at low turbulence intensity commenced near separation of the laminar boundary layer and the empirical correlation of Abu - Ghannam and Shaw (1980) was not suitable to predict the onset of natural transition on the pressure (concave) surface.

In order to investigate the effect of high subsonic or supersonic Mach number on the heat transfer rate, Martin et al. (1978), Dunn and Stoddard (1979), Nicholson et al. (1982), Consigny and Richards (1982), Dunn and Hause (1982), Dunn et al. (1984a, 1984b), Arts and Graham (1985) and Guenette et al. (1989) applied transient methods using shock tunnel facilities or a blowdown turbine tunnel to study the turbine blade heat transfer distributions. These facilities provide well-defined flow conditions and the ability to simulate the test conditions of a real engine and to measure real-time heat transfer response. Typical outlet Mach number ranges from approximately 0.7 to 1.18. The shock wave induced on the suction surface has little effect on the local heat transfer rate for the high turbulent level case (Consigny and Richards, 1982). To simulate a full-scale engine, Dunn and Hause (1982) found the stator heat transfer rate for the full-stage case was about 20% higher than that for the stator-only case.

Hippensteele et al. (1985, 1987) applied the liquid crystal technique to measure the local heat transfer coefficient on a turbine airfoil. Their results showed some spanwise periodic temperature patterns on the suction surface, possibly caused by straw straighteners. From visualization results using yellow pigmented oil, they observed a laminar separation bubble formed on the pressure surface in the region just behind the leading edge. This separation bubble could be suppressed by increasing the flow inlet angle (Consigny and Richards, 1982).

Experimental measurements were conducted in long run-time cascade facilities, by Blair (1974), York et al. (1979), Graziani and Blair (1980), Nealy et al. (1984). Local heat transfer coefficients could be measured under steady-state conditions. Two studies by Sato and Takeishi (1987) and Sato et al. (1987) presented comprehensive local heat transfer results using electrically heated isothermal vanes in a low-speed wind tunnel. The effect of film cooling on the heat transfer process was also considered in these studies.

All of the studies noted above use heat transfer instrumentation. Kan et al. (1971) used a naphthalene sublimation technique to investigate the mass (heat) transfer from a turbine blade embedded in the two-dimensional flow region at different values of pitch-chord ratio, flow inlet angle, Reynolds number and main stream turbulence intensity. They showed that early transition occurred on the pressure surface when the flow inlet angle was small, but it became unclear where transition occurred when the flow inlet angle approached 40°. Chen and Goldstein (1988) also presented detailed mass transfer results on both surfaces of a turbine blade using the naphthalene sublimation technique. Both studies agree well in the trend of the mass transfer distribution.

Due to a low aspect ratio of the first stage rotors or vanes, it is unrealistic to ignore the influence of the endwall on the flow field as well as the convective transport process. Sharma and Bulter (1987) and Yamamoto (1987) proposed some numerical schemes to predict endwall losses and secondary flows in turbine cascades. Detailed experimental investigations of the production and development of the secondary flows were presented in studies by Yamamoto (1987) and Bario et al. (1982). Sonoda (1985) used kerosene vapor to visualize the flow field in the blade passages. Although the approaching boundary layer flow in his study was laminar, the evolution of vortices was clearly captured. Hodson and Dominy (1987a) used a mixture of fluorescent powder and silicone oil to trace the limiting streamlines on both suction and pressure surfaces of a low-pressure turbine blade. In their study, a two-dimensional separation bubble near the stagnation line was observed on both pressure and suction surfaces. Furthermore, the laminar boundary layer on the suction surface underwent separation, reattachment, and possibly transition, near the trailing edge, but this separation disappeared at higher inlet Reynolds numbers, Re_1. After studying the surface oil flow pattern, they concluded that the strengths and locations of the vortices were mainly affected by the approaching boundary layer and the blade loading instead of the inlet

Reynolds number. By changing the incidence from +7.2° to -53.3° Yamamoto and Nouse (1988) showed the effect of incidence on the three-dimensional flows, blade loading at tip, and overall pressure loss in a linear rotor cascade. A detailed description of secondary flows in turbine blade passages can be found in a review of many earlier studies by Sieverding (1985).

Few studies are available on the effect of secondary flows on blade heat transfer. Walker and Markland (1965), Graziani and Blair (1980), and Sato et al. (1987) showed that the heat transfer rate on the suction surface was strongly affected by the secondary flows, especially in the region near the endwall. On the pressure surface, little effect of the secondary flow is observed. These measurements, however, were conducted using test blades with limited numbers of heat flux gauges or thermocouples and might not present the whole picture of the heat transfer distribution.

Besides experimental studies, many computational codes have been proposed to evaluate the heat transfer rates to gas turbine blades. Daniel and Browne (1981) tested five different computer programs which used different methods to model the turbulence quantities. The predictions are in good agreement with experimental data only in the laminar (leading edge) region and the fully turbulent region. Winstanley et al. (1981) used three different numerical schemes to predict the heat transfer distribution. Their results overestimated the surface heat transfer when compared with experimental data. Wang et al. (1985) incorporated a k-ε turbulence model with STAN5 to predict the heat transfer rate around turbine airfoils. Predicted results show a better agreement with the experimental data for the pressure surface than those for the suction surface. Some experimental studies, mentioned earlier, also compared numerical predictions with measured results. Two computational codes, two-dimensional parabolic boundary layer code (STAN5) and three-dimensional viscous code (NANCY), have been often used. Neither has achieved great success. This is attributed to inaccurate models for turbulence and the detailed flow conditions of the mainstream and blade surface boundary layer flow.

In the present study, a naphthalene sublimation technique is used to study the mass transfer coefficient instead of the heat transfer coefficient. Since the secondary flow over the suction surface is much more complex than that over the pressure surface, the present study only focuses on measuring the mass transfer distribution over the suction surface of a turbine blade. With the help of an automated data acquisition system, the mass transfer coefficient at several thousand locations over the test surface can be obtained for a single run and this can provide a detailed mass transfer distribution. This technique not only has high resolution, but also avoids heat conduction in the blade wall which can mask out variations in convective transport. Values of the heat transfer coefficient can be evaluated from the measured mass transfer coefficient by applying the heat/mass transfer analogy.

EXPERIMENTAL APPARATUS

Wind tunnel and test section

The mass transfer experiments are conducted in the same open-circuit, low speed wind tunnel that has been described in earlier film cooling studies (Ito et al., 1978). The configuration of the wind tunnel and the planar cascade is shown in Figure 1. Three of seven threaded instrument holes ahead of the cascade are used to insert a total pressure tube, a static pressure tap, and a thermocouple. The approaching free-stream velocity, U_1, is measured at the third threaded hole (at the right-hand side of the center hole), 145 mm upstream of the leading edge of the cascade. A slot in the top endwall located immediately after the cascade is used to install a total pressure tube and a static pressure tap for determining the cascade exit velocity, U_2.

The planar cascade consists of six scaled-up CF6-50 blades made of aluminum. Figure 2 shows the geometry of the blade. It has a chord length of 169.1mm and its leading edge is an ellipse with a ratio of major to minor axis of 1.16. Coordinates of the surface profile of the test blade and parameters of the cascade geometry are given in Table 1 and Table 2, respectively. Each of the center two blades (the third and fourth blades counted from the top of the cascade in Figure 1) of the cascade has three components: a bottom hollow section, a middle solid section and a top supporting section. These three sections are held tightly together by two threaded bars. Lengths of the bottom, middle and top sections are 600 mm, 171.5 mm, and 171.5 mm, respectively. During a mass transfer measurement, the middle solid section of the blade is replaced by the test piece, coated with naphthalene. Four dowel pins are used to ensure the same installation alignment for every mass transfer measurement.

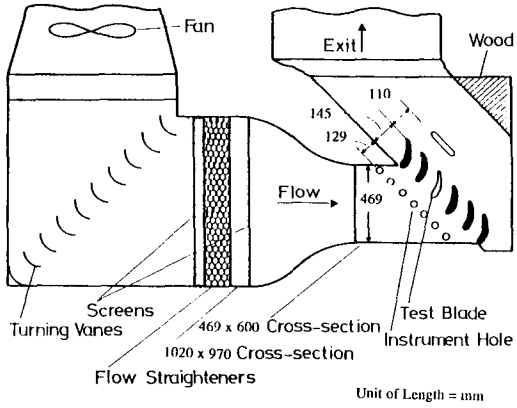

Figure 1 A schematic view of the wind tunnel and cascade

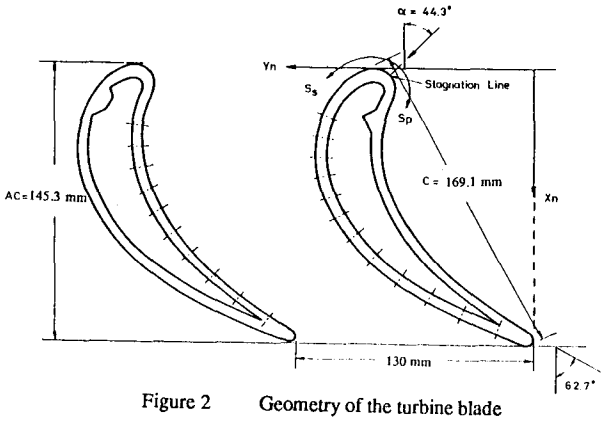

Figure 2 Geometry of the turbine blade

TABLE 1
COORDINATES OF THE BLADE CONTOUR AND LOCATIONS OF THE PRESSURE TAPS (see Figure 2)

Concave Side			Convex Side		
X_n/AC	Y_n/AC	S_p/C	X_n/AC	Y_n/AC	S_s/C
			.01	.55	.007
			.000	.583	.037
.075	.521	.058	.005	.6147	.061
.15	.5478	.138	.045	.683	.133
.225	.565	.193*	.175	.7737	.270*
.3	.567	.257*	.25	.7948	.337*
.375	.555	.323*	.325	.7998	.402*
.45	.5306	.391*	.4	.7909	.467*
.525	.4928	.463*	.475	.768	.534*
.6	.4429	.540*	.55	.731	.606*
.675	.3775	.624*	.625	.6774	.686*
.75	.2948	.722*	.7	.6022	.777*
.825	.1953	.829*	.775	.5025	.884*
.9	.845	.944*	.84	.3912	.995*
.98	.0	1.045	.9	.2679	1.113*
			.96	.1302	1.242*
			1.0	.0220	1.341

* indicates locations of the pressure taps

TABLE 2 - CASCADE GEOMETRY

Number of blades	6
Chord length, C (mm)	169.1
Axial Chord, (mm)	145.3
Aspect Ratio	3.548
Pitch, (mm)	131.1
Inlet Angle	44.3^{o}
Exit Angle	62.7^{o}
Leading edge radius to chord ratio	0.054

Test blade

The test blade consists of two smooth end pieces and a roughened piece in the middle. All three pieces are made of aluminum. The center part of the test blade, coated with solid naphthalene during a mass transfer measurement, has a span of 165.1 mm. Both end portions have the same contour as the blades of the cascade. The surface of the roughened section is approximately 1.63 mm deep as compared with the end pieces. Eleven grooves are also cut into each surface of the roughened blade in order to hold naphthalene better. Two thermocouples are installed at the central region of this roughened section, one on the pressure side and the other on the suction side.

Velocity and Pressure Measurement

The velocities at different streamwise locations over a turbine blade are determined by measuring the dynamic pressure between a total pressure tube located upstream of the cascade and static pressure taps on the blade. The value of the dynamic pressure is measured with a micromanometer, a Microtector made by Dwyer Company, which has resolution of 0.001 inch and a range of 2 inches water head.

The static pressure distribution over the blade surface is measured relative to a barometer pressure with the same micromanometer. Since the blades with pressure taps can be moved up and down through the walls, the pressure distribution at different elevations from the wall can be determined.

Data-acquisition system

An automated four-axis data acquisition system is used to measure the sublimation depth over the test blade naphthalene surface. This system can fulfill many strict requirements of a mass transfer measurement, summarized as precise positioning, accurate surface elevation reading, and fast data acquisition (2500+ data points within a one hour period). It includes a four-axis positioning stand, a depth gauge, an IBM-XT, and a motor-controller system. A detailed description of this system can be found in a study by Chen and Goldstein (1988).

The central part of the data acquisition system is a four-axis positioning stand, shown in Figure 3. The probe (LVDT) can be moved independently in three directions, X,Y, and Z_T. The test piece can be rotated around an axis in the θ direction. The main function of this stand is to align the test piece and to move the depth gauge accurately and quickly on the naphthalene surface (S_p -Z_T or S_S - Z_T). Since the local mass transfer rate is determined from the difference in naphthalene surface profiles at the same location measured before and after exposure to the flow, the test piece must be precisely installed on the positioning mechanism.

PROCEDURE AND TEST CONDITIONS

Experimental procedure

After a smooth naphthalene layer is cast on the test blade, the naphthalene surface profile is measured at designated locations before the test blade is installed in the wind tunnel. Then the test blade is put into a sealed plastic box to prevent sublimation due to natural convection. It is placed in the wind tunnel and exposed to the air-stream for a period of 30 - 45 minutes, depending on the test conditions. Meanwhile, the readings of the thermocouples are recorded. Since the naphthalene vapor pressure is susceptible to changes in temperature, it is important to keep a steady free-stream

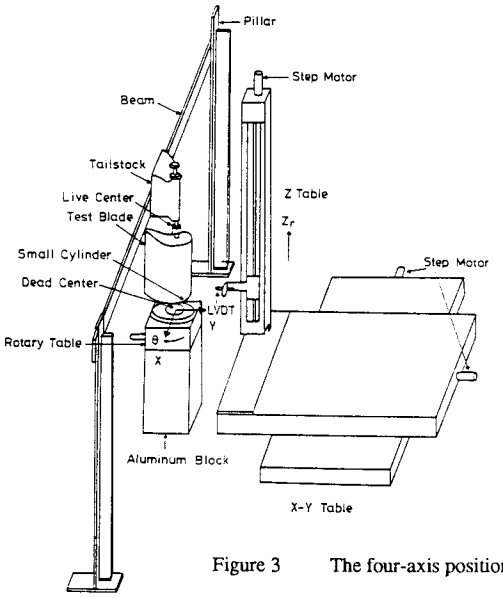

Figure 3 The four-axis positioning stand

temperature. Finally, the test blade is removed from the wind tunnel and installed back in the positioning mechanism. Readings of the second surface profile are at the same locations as in the first measurement. The change in naphthalene thickness during exposure in the flow is determined from the difference of these surface profiles.

The mass transfer coefficient is evaluated from the measured naphthalene sublimation loss,

$$h_m = \dot{m} / (\rho_{v,w} - \rho_{v,\infty}) = L_{sb}\cdot\rho_s / [(\rho_{v,w} - \rho_{v,\infty})\,\Delta t] \quad (1)$$

In the free-stream, $\rho_{v,\infty}$ is equal to zero and

$$h_m = L_{sb}\cdot\rho_s / (\rho_{v,w})\,\Delta t \quad (2)$$

The mass transfer coefficient can be nondimensionized as the mass transfer Stanton number

$$St_m = h_m / U_1 \quad (3)$$

or the Sherwood number

$$Sh = h_m C / D \quad (4)$$

where D is the diffusion coefficient of naphthalene in air. A discussion of the value of the diffusion coefficient is given in a study by Chen (1988).

To compare the present results with direct heat transfer measurements, a heat/mass transfer analogy is applied. The analogy between heat and mass transfer process was discussed by Eckert (1976). The definition of the heat transfer coefficient can be expressed as

$$h = q / (T_w - T_\infty) \quad (5)$$

Correspondingly, the mass transfer coefficient is defined as

$$h_m = \dot{m} / (\rho_{v,w} - \rho_{v,\infty}) \quad (6)$$

At the same flow conditions, the sublimation mass transfer system is equivalent to a heat transfer system with a constant wall temperature boundary condition. Empirical correlations are commonly applied to correlate the heat and mass transfer coefficients when Sc and Pr are not equal. Often power law relation is used,

$$Nu = C_1 Pr^n Re^p \quad (7)$$

and

$$Sh = C_1 Sc^n Re^p \quad (8)$$

For the same Reynolds number

$$\frac{Nu}{Sh} = \left[\frac{Pr}{Sc}\right]^n \quad (9)$$

If the Stanton number and the mass transfer Stanton number are to be used,

$$\frac{St}{St_m} = \left[\frac{Pr}{Sc}\right]^{n-1} \quad (10)$$

For air the Prandtl number is approximately 0.7 and the value of the Schmidt number by naphthalene in air is between 2.0 and 2.5, depending on the flow conditions and the temperature at the naphthalene surface. In Equations 9 and 10, n is an empirical constant; its value is taken as 1/3 in the present study. It should be noted that relationships such as Equations 7-10 are not required if only relative values are intended such as comparison of transport in the end-wall region to that on the blade in the two-dimensional flow.

Test Conditions

The test conditions established for the experiments are given in Table 3. For measurements in the two-dimensional flow region, the exit Reynolds number was either 122,000 or 171,000. When the effect of secondary flows was considered, the approaching displacement thickness on the endwall (measured 145 mm upstream of cascade) was changed from 2.13 mm (case 1) to 3.18 mm (case 3) at the same exit Reynolds number, Re_2 = 171,000. For the data run in the two-dimensional flow region, the active naphthalene area of the test blade extends from midspan of the test section to 131.3 mm from the endwall. For measurements in the three-dimensional flow region, the test blade is moved into the location at which 1.5 mm of naphthalene is embedded into the top endwall.

TABLE 3 - TEST CONDITIONS

	Case 1	Case 2	Case 3
U_1(m/sec.)	10.45	7.33	10.45
U_2(m/sec.)	17.18	12.05	17.18
Re_1	104,000	73,000	104,000
Re_2	171,000	122,000	171,000
d_w(mm)	1.59	1.59	3.76
δ_1 (mm)	2.13	2.4	3.18
δ_2 (mm)	1.51	1.69	2.25
H	1.41	1.42	1.41
Tu(%)	1.31	1.27	1.31

Based on the method proposed by Kline and Mclintock (1963), the uncertainty in h_m of the present study is about 4.9%. A detailed discussion on the estimation of the uncertainty was presented by Chen and Goldstein (1988).

RESULTS AND DISCUSSIONS

Velocity and pressure distribution

The variation of free-stream velocity, U/U_2, over both surfaces of the blade is presented in Figure 4. Predicted values of U, supplied by General Electric, compare well with measured data (Ito et al., 1978). On the suction side, the velocity rapidly increases up to $1.15U_2$ at $S_s/C \approx 0.05$, indicating a strong acceleration. After the strong acceleration, the velocity is almost uniform along the whole suction surface. On the pressure surface, a strong rapid acceleration around the leading edge is followed by a region of deceleration till $S_p/C \approx 0.3$ following which the flow undergoes a strong acceleration as S_p increases further. In the accelerated region, the pressure gradient parameter $\frac{\mu}{\rho U^2}\frac{dU}{dS_p}$ is about 16 x 10^{-6} which is considerably greater than the commonly accepted value (2 x 10^{-6}) above which relaminarization can occur. The difference between the present data and earlier results indicates that the normalized velocity distribution is slightly affected by a change in the exit Reynolds number. Note that the locations marked "separation" and "reattachment" on Figure 6 were inferred from the mass transfer measurement.

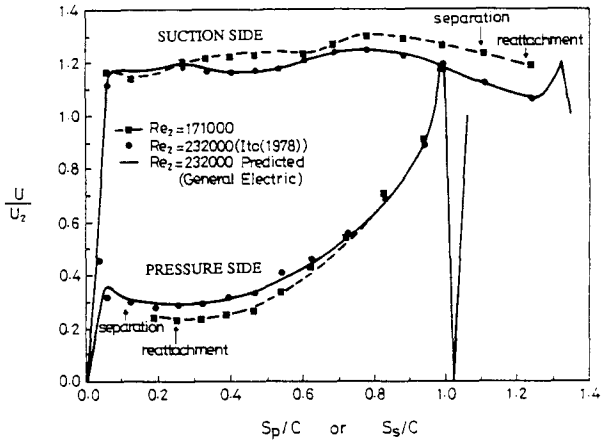

Figure 4 Normalized velocity distribution along the blade surface

Figure 5 shows contours of the static pressure coefficient on the suction surface at Re_2 = 171,000. The measurement area is from the endwall (Z = 0) up to Z/C = 0.7 and data at Z/C = 0.7 were used to obtain the free-stream velocity, U, shown in Figure 4. Note that data near the leading edge are not available due to the absence of pressure taps. The effect of secondary flows is quite significant. A two-dimensional flow region can only be found in the region Z/C > 0.6. For the region 0.6 > Z/C > 0.3, the flow accelerates from the leading edge toward a low pressure zone (C_{ps} = -2.9) located near S_s/C = 0.72. After the low pressure zone, a steep adverse pressure gradient causes a two-dimensional laminar separation which is confirmed by the mass transfer measurements. The two-dimensional separation was also observed in several studies on different turbine blades [e.g. Hodson and Dominy, 1987a and Hoheisel et al., 1987]. In the region from $S_s/C \approx 0.2$ to 0.6, a pressure gradient in the spanwise direction drives both the suction side horseshoe vortex and the passage vortex upward, away from the endwall.

Flow field

Measurements and flow visualizations have been extensively employed to study the flow field around a turbine blade. Although the flow field has a strong dependence on the incidence angle, flow inlet angle, Reynolds number, characteristics of the oncoming boundary-layer flow and the blade profile, the qualitative trends are quite general. The boundary-layer flow in the two-dimensional flow region, shown in Figure 6, is summarized from studies conducted by

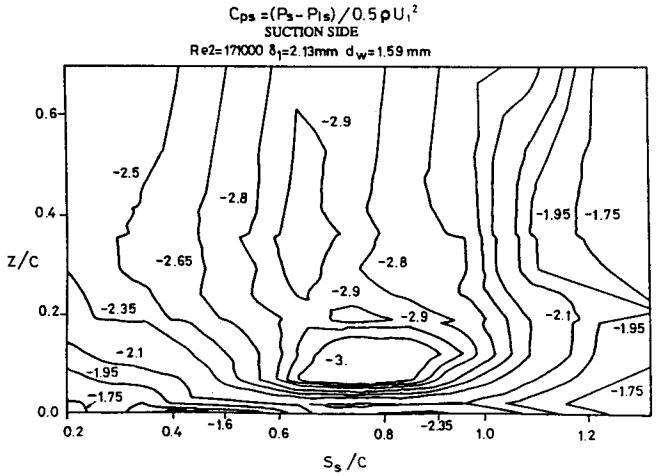

Figure 5 Suction blade surface pressure coefficient contour

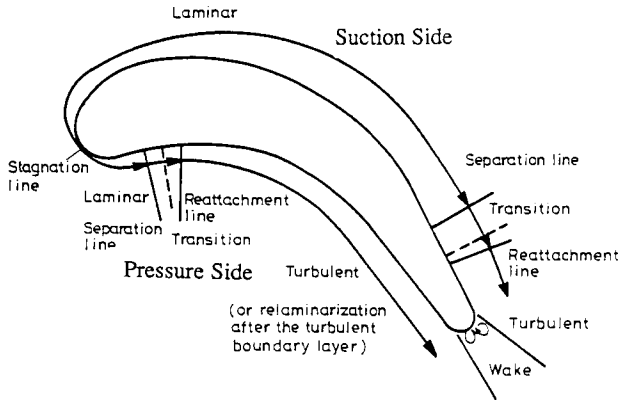

Figure 6 Boundary layer over a turbine blade in the two-dimensional region

Hodson and Dominy (1987b), Hoheisel et al. (1987), and Nicholson et al. (1982). On the suction side, a laminar boundary layer grows from the stagnation line. Hodson and Dominy (1987b) observed that the laminar boundary layer proceeds through separation, transition and reattachment after which the flow becomes fully turbulent near the trailing edge. This separation bubble, near the trailing edge, is also indicated by the mass transfer measurement in the present study. Vortices shed from the trailing edge are present in the wake region. The flow field, on the pressure surface, is also indicated in Figure 6. The laminar boundary layer develops from the stagnation line and a separation bubble forms near the leading edge. In the separation bubble, a transition occurs and develops into a fully turbulent boundary layer. The turbulent boundary-layer flow, subjected to a strong acceleration, might relaminarize.

Based on earlier studies, the secondary flows in the three-dimensional flow region within the blade passage are schematically presented in Figure 7 from Goldstein and Spores (1988). When the incoming boundary layer on the endwall approaches the blade, it is subjected to an adverse pressure gradient and starts to roll up to form a horseshoe vortex. Ahead of the leading edge of the blade, S_1-S_2 is the separation line of the horseshoe vortex and the two legs of the horseshoe vortex are marked as vortices V_{sh} and V_{ph}. The leading edge corner vortex, driven by the horseshoe vortex, forms at the corner of the leading edge and rotates an opposite direction to the horseshoe vortex. Separating from the leading edge, the suction and pressure side leading edge corner vortices are marked as vortices V_{sLc} and V_{pLc}, respectively. A verification of this intense leading edge corner vortex from the mass transfer results will be shown in a later section.

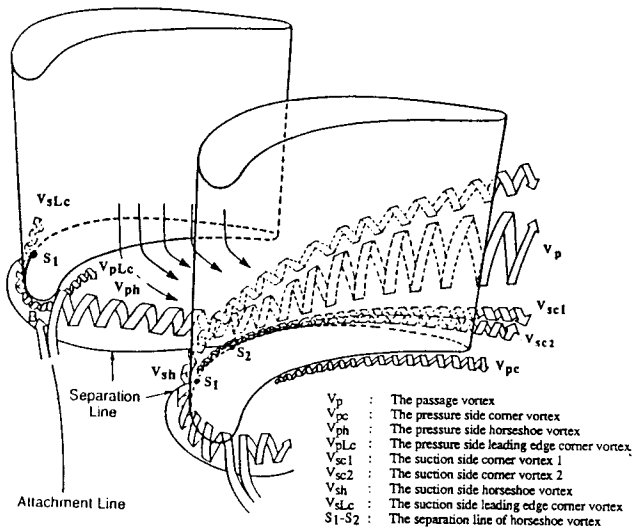

Figure 7 Diagrams of turbine blade vortices

The strong pressure gradient in the blade passage is the main driving force of the complex secondary flows. It affects the path of the low momentum flow, on the endwall as well as the secondary flows in the passage. It is also responsible for the overall downflow (towards the endwall) on the pressure surface and upflow on the suction surface. When both the suction side leading edge corner vortex and horseshoe vortex enter the blade passage, they experience the strong transverse pressure gradient and both vortices are kept close to the suction surface.

As the suction side horseshoe vortex travels along the suction surface toward the trailing edge, it moves away from the endwall towards the midspan and downstream to the separation bubble. When the suction side horseshoe vortex moves away from the endwall, its separation line is at S_1, shown in Figure 7. Hodson and Dominy (1987a) indicate that the direction of the rotation of the flow in the separation bubble is opposite to that of the suction side horseshoe vortex; as a result, the vorticity of this vortex decreases. As to the leading edge corner vortex, after it is forced toward the suction surface, its path is not easily traced nor do earlier studies have a clear view of it.

The pressure (concave) side horseshoe vortex leg, driven by the strong transverse pressure gradient, moves away from the pressure surface and towards the suction surface of the adjacent blade. During the transverse movement, it becomes a major component of the passage vortex (V_p) that entrains fluid from the endwall boundary layer, as well as the main stream. After the passage vortex reaches the suction surface of the adjacent blade, it moves away from the endwall towards the midspan as it travels along the suction surface towards the trailing edge. The location, S_2, is shown in Figure 7 and indicates the extrapolation of the separation line of the passage vortex at the suction surface.

Using the kerosene oil vapor to visualize the flow field, a pair of suction side corner vortices (V_{sc1} and V_{sc2}) were observed by Sonoda (1985). This observation was also indicated by Goldstein and Spores (1988) from regions on the endwall with high mass transfer rate, caused by these intense vortices. In the present study, the mass transfer results indicate one suction side corner vortex (V_{sc1}) starts behind the location of S_1 and another (V_{sc2}) forms behind the location S_2. Over the pressure surface, the flow is relatively simple. At the endwall/pressure-side corner, a pressure side corner vortex (V_{pc}) is formed due to the downflow on the pressure surface.

To help in identifying distinct regions affected by the secondary flows over the suction surface, Figure 8 shows both the separation line and the reattachment line of the secondary flows. The path of these lines is determined from the mass transfer results. It has been reported that a low transfer rate is associated with the

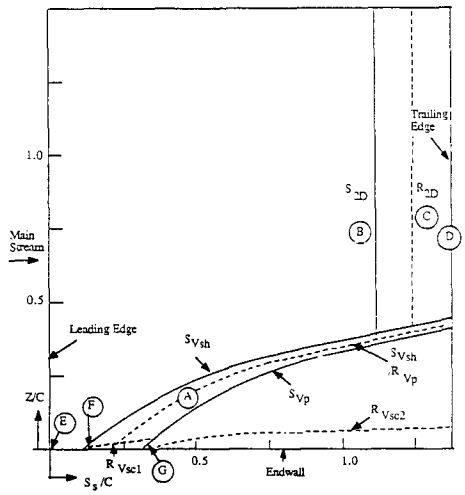

Figure 8 Limiting streamline pattern on the suction surface of the test blade

separation of the boundary layer and a high transfer rate with the reattachment of the flow (e.g. Consigny and Richards, 1982). As shown in Figure 8, areas of interest are labelled A through G, interpreted from the mass transfer results in later sections, and the reattachment and separation lines of the flow are denoted by R and S, respectively. The separation lines (S_{Vsh} and S_{Vp}) indicate the evolution of the suction side horseshoe vortex and the passage vortex on the suction surface. Between these two separation lines, a reattachment line, R_{Vsh}/R_{Vp}, is observed (cf. Hodson and Dominy, 1987a). As the suction side horseshoe vortex moves toward the trailing edge, it encounters the two-dimensional separation bubble which is defined by the lines S_{2D} and R_{2D}. The reattachment lines (R_{Vsc1} and R_{Vsc2}) associated with the suction side corner vortices are also shown.

Leading Edge Mass Transfer on a Turbine Blade

Figure 9 shows the blade stagnation Nusselt number in the two-dimensional flow region as a function of the Reynolds number, Re_d. Values of the Nusselt number from the present measurement are determined from the Sherwood number using the empirical correlation (Equation 9) with Pr = 0.7 and Sc = 2.04. It should be noted that some recent (as yet unpublished) studies indicate a somewhat higher value of Sc.

The present measured results are compared, on Figure 9, to two correlations for heat transfer from a circular cylinder in a cross flow from Kestin and Wood (1971) and Lowery and Vachon (1975). The values from these two correlations are calculated at Tu = 1.31%

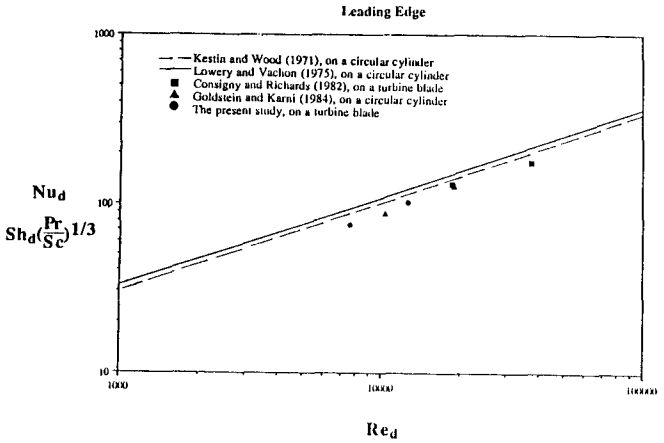

Figure 9 A comparison of the leading edge heat transfer in the two-dimensional flow region

which is the turbulence level in the present study. Data points also include heat transfer results from Consigny and Richards's (1982) study for Tu = 0.8% and mass transfer results from Goldstein and Karni's (1984) study for Tu = 0.43%. These measured results are about 8% lower than values predicted by the Kestin and Wood (1971) correlation.

Mass transfer results in the two-dimensional region

Figure 10 provides a comparison of the variation of the mass transfer Stanton number for two exit Reynolds numbers, 171,000 and 122,000. Though the values of mass transfer Stanton number are higher at smaller exit Reynolds number, the general trends of the mass transfer distribution is similar for the two flows. It is interesting to note, as shown in Figure 10, that the maximum mass transfer does not occur at the stagnation line. This is also observed for flows over a heated ellipse (Ota et al., 1983) and in a study of the heat transfer over a turbine blade with an elliptic leading edge (Art and Graham, 1985).

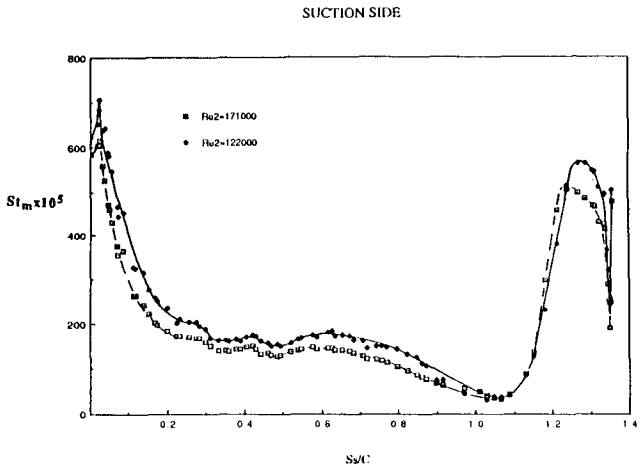

Figure 10 A comparison of curvilinear distribution of the average mass transfer Stanton number on the suction surface between two different Reynolds numbers

After the mass transfer reaches the peak value at $S_s/C \approx 0.01$, it drop off rapidly. This sharp drop ends approximately at $S_s/C \approx 0.27$, after that a varying mass transfer distribution, with two modest local peaks, at $S_s/C \approx 0.42$ and $S_s/C \approx 0.62$, is observed. The variation in curvature and the resulting pressure gradient along the suction surface apparently have a significant effect on the mass transfer distribution. At $S_s/C \approx 1.08$, the mass transfer rate reaches a minimum, probably due to laminar separation. The rapid increase of the mass transfer in the region from $S_s/C \approx 1.08$ to 1.18, after the separation, may indicate a progression through transition and reattachment. The exact location of the onset of transition within the laminar separation bubble cannot be determined from the mass transfer distribution.

Following reattachment, the mass transfer rate falls sharply. In the trailing edge zone, a rapid increase in the mass transfer rate to a value slightly less than that in the leading edge region is observed. The high transport rate is probably due to the vortices shed from the trailing edge. This implies that an effective cooling system must be applied in this region. A comparison with a heat transfer study by Consigny and Richards (1982) is presented in Figure 11. Their exit Reynolds number 1.5×10^6 is much higher than Re_2 of the present study. The equivalent values of Nusselt number for the present study are evaluated from the Sherwood number using Equation 9; $Nu/Re_2^{0.5}$ is plotted to allow a more reasonable comparison.

From Figure 11, it is clear that the present technique is capable of showing more detail in the transport coefficient variation than a typical heat transfer experiment. Although the blade geometry is quite different in the two studies, the results of Consigny and Richards' (1982) are qualitatively similar to those of the present work.

Mass transfer results in the three-dimensional region

The influence of the endwall on the mass transfer rate along the suction surface is significant. The measurements are conducted at two values of the displacement thickness with the same free-stream velocity. The inlet displacement thickness, δ_1, is 3.18mm and 2.13mm for the "thick" and the "thin" boundary layers, respectively.

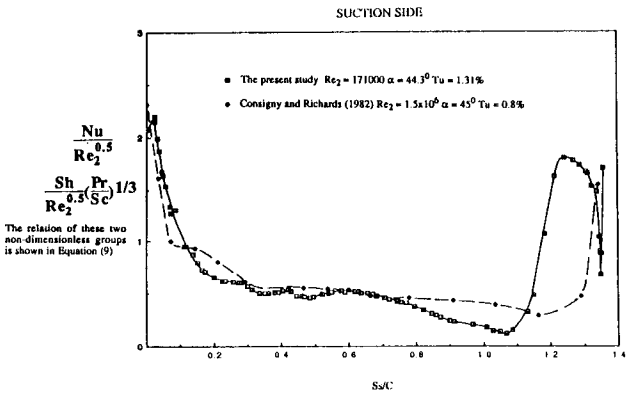

Figure 11 A comparison of curvilinear distribution of the average Nusselt number on the suction surface between the present study and the study by Consigny and Richards (1982)

Stanton number contours for the two displacement boundary layer thicknesses are presented in Figures 12 and 13, respectively. The difference between both contour plots is small. This indicates little influence of boundary-layer thickness on the blade mass transfer over the range studied. Enlargements of Figures 12 and 13 in the region from $S_S/C = 0.0$ to 0.4 near the endwall are presented in Figure 14 and 15, respectively.

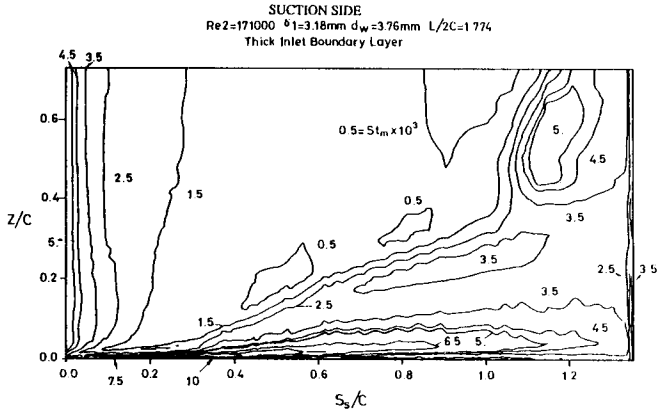

Figure 12 Suction surface Stanton number contours for case 3 (see Table 3)

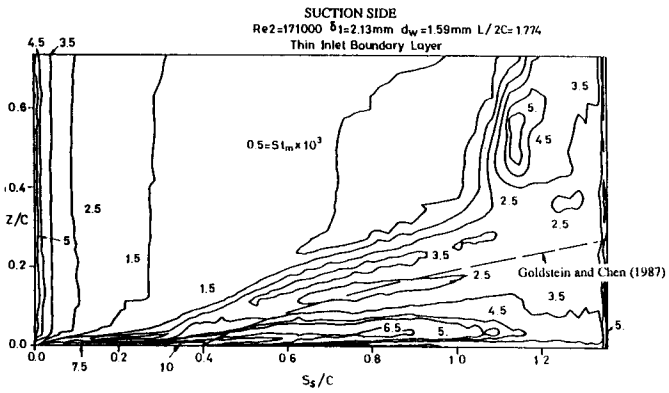

Figure 13 Suction surface Stanton number contours for case 1 (see Table 3)

Figures 12 and 13 show the strong three-dimensional flow field greatly influences the suction surface mass transfer except in the leading edge region, where three-dimensionality is confined to a narrow region very close to the endwall. Near the stagnation line of a circular cylinder, Goldstein and Karni (1984) also observed that the horseshoe vortices only affect the mass transfer in the region very close to the endwall. Complex mass transfer patterns are observed and mass transfer levels are higher than two-dimensional values. In the region from $S_S/C \approx 0.9$ to the trailing edge ($S_S/C = 1.355$), the flow is essentially three-dimensional over the whole measurement region ($Z/C < 0.77$).

The variation in mass transfer results is closely related to limiting streamline pattern, shown in Figure 8. When the suction side horseshoe vortex lifts off the endwall as it moves towards the trailing edge, its separation line ($S_{V_{sh}}$), shown in Figure 8, can be traced approximately as a diagonal line, with a St_m of 0.0015 in the contour plots (Figures 12 and 13). Underneath this diagonal line, the value of St_m increases from 0.0015 to 0.0035 along the spanwise direction (Z) and this increase is due to the reattachment line, $R_{V_{sh}}/R_{V_p}$, in Region A.

When the passage vortex moves away from the wall and travels toward the trailing edge, the separation line of the passage vortex (S_{V_p}) creates an area of low mass transfer with a Stanton number of 0.0025, shown in Figure 12. Near the endwall, the contour lines are packed within a narrow region from the wall and most of them can not be distinguished. This indicates the presence of large gradients in the Stanton number occurring in this region, a result of the intense suction side leading edge corner vortex and the suction side corner vortices. The strip with $St_m = 0.0065$ is due to the effect of the reattachment line ($R_{V_{SC2}}$). Along the curvilinear direction (S_S) and further away from the wall ($Z/C \approx 0.6$), the mass transfer drops sharply from $St_m = 0.005$ at the leading edge to 0.0005 at $S_S/C \approx 1.0$. The low mass transfer zone, Region B, is a result of the laminar separation. Further downstream, the mass transfer increases up to a value of St = 0.005, indicating the reattachment of the boundary-layer flow (Region C). Downstream of the reattachment, the decrease in the mass transfer is expected as the boundary-layer flow becomes fully turbulent; and finally the mass transfer rate increases again up to a value of $St_m = 0.0035$ in the trailing edge region (Region D).

The dashed line, shown in Figure 13, is the upper boundary of the unprotected region in which the coolant ejected from two rows of cooling holes located at $S_S/C \approx 0.208$ and 0.243 is absent as found by Goldstein and Chen (1987). Their conclusion that this unprotected region is due to the presence of the passage vortex is confirmed by the present mass transfer results measured in the same cascade. Figure 13 reveals that the dashed line passes through a low mass transfer zone with a value of $St_m = 0.0025$ which is caused by the separation line of the passage vortex.

Three peaks with values of St_m = 0.0075 or 0.01 can be seen in both Figures 14 and 15. These peaks indicate the inception points of the leading edge corner vortex (at S_s/C = 0.0 (Region E)), the suction side corner vortex 1 (V_{sc1} at S_s/C = 0.095 (Region F)) and the suction side corner vortex 2 (V_{sc2} at S_s/C = 0.35 (Region G)). When the suction side horseshoe vortex moves away from the endwall at S_1 (see Figure 7), it creates a low mass transfer zone between two contour lines with a value of St_m = 0.0035 near Z/C ≈ 0.005 and S_s/C ≈ 0.05, shown in Figures 14 and 15. The suction side corner vortex 1 is formed as a result of the high angle of attack of the surface streamlines onto the suction surface (Hodson and Dominy, 1987a) and originates near the point where the suction side horseshoe vortex meets the suction surface. When the boundary-layer flow on the endwall of the blade passage is driven by the pressure gradient from the pressure surface toward the suction surface, the suction side corner vortex V_{sc2} is formed by both the separation of the boundary-layer flow near the suction surface and the high angle of attack of the passage vortex. This suction side corner vortex originates near the point S_2 (see Figure 7) where the passage vortex encounters the suction surface.

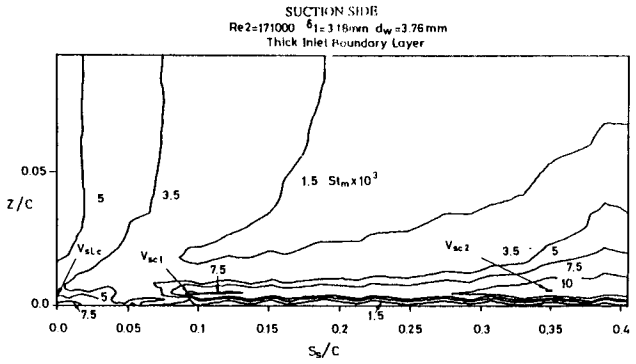

Figure 14 Enlargement of Figure 12 in the leading edge region near the endwall

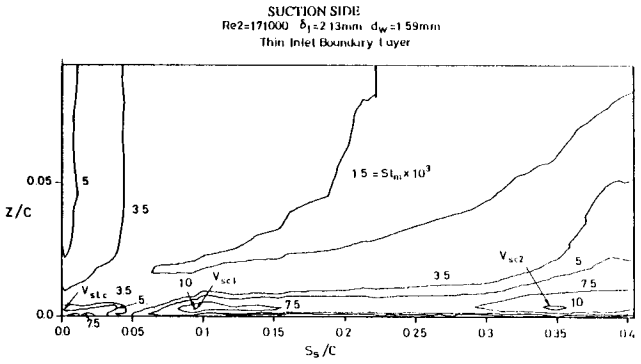

Figure 15 Enlargement of Figure 13 in the leading edge region near the endwall

Figure 16 shows the spanwise Stanton number distributions at three different values of S_s. Enlargements of Figure 16 for locations near the endwall are presented at Figure 17. In general, major trends of the Stanton number to both boundary layer cases are close enough that the St_m peaks occur at approximately the same values of Z/C. The dominant peak with St_m ≈ 0.01 (Figure 17(a)) is the highest on the suction surface. This peak is a result of the intense suction side corner vortex V_{sc2}. At the larger δ_1 studied, the dominant peak is slightly further from the endwall. Figure 16(c) shows the secondary peak (St_m ≈ 0.0036) at Z/C ≈ 0.12 for large S_s/C; this is a result of the reattachment line (R_{Vsh}/R_{Vp}) between S_{Vp} and S_{Vsh}.

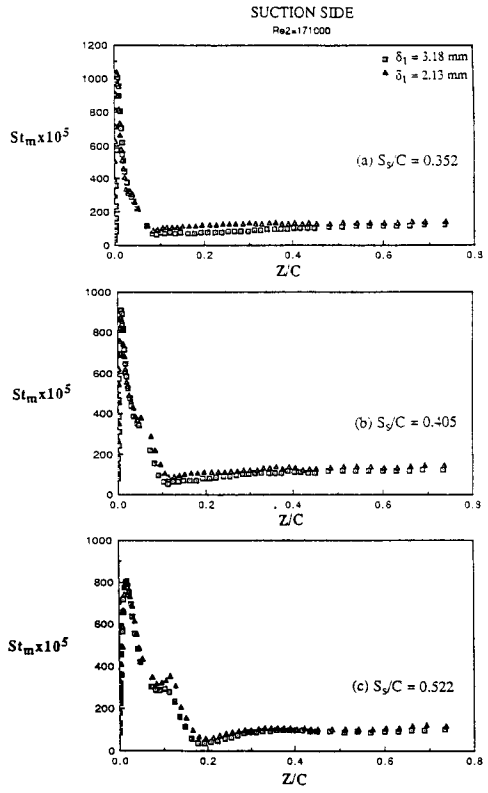

Figure 16 A comparison of spanwise distribution of local Stanton number on the suction surface at selected curvilinear locations between cases of two different displacement thicknesses

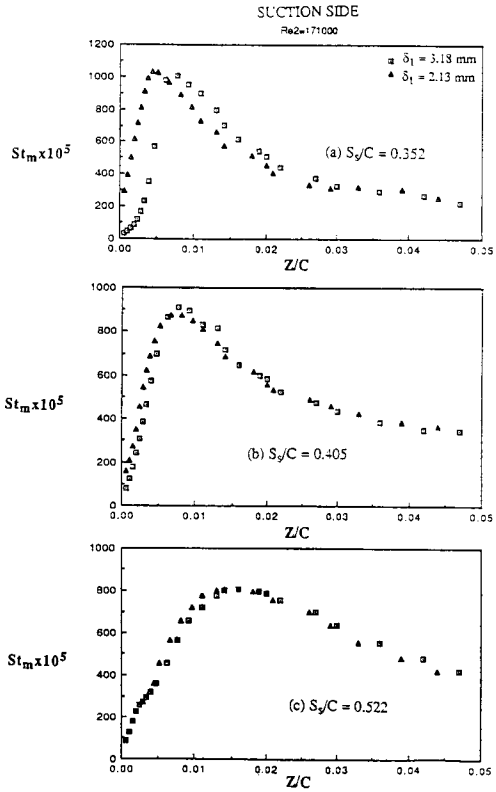

Figure 17 Enlargement of Figure 16 in the region near the endwall

Figure 18 shows the spanwise variation of the curvilinear average (along curvilinear, S_S, direction) Stanton number over the whole chord from $S_S/C = 0$ to $S_S/C = 1.355$ at two different inlet boundary layer thicknesses. The average Stanton number from measured data points in the two-dimensional region is shown as the dashed line (It is independent of δ_1.). The mass transfer rate is higher for the thicker boundary layer except in the region very close to the endwall. The average mass transfer rate (St_m) near the endwall is much larger than that in the two-dimensional flow region.

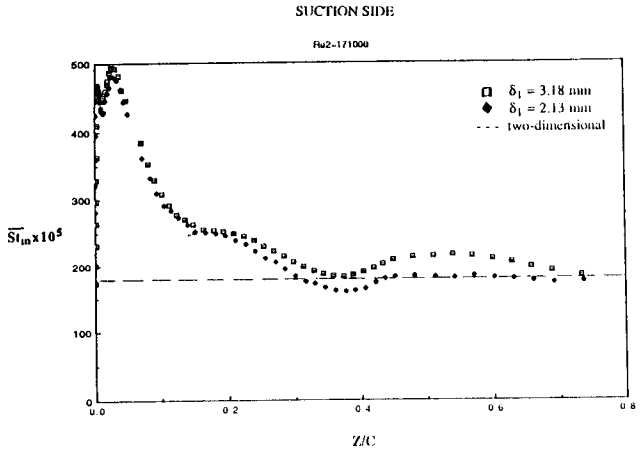

Figure 18 A comparison of spanwise distribution of the average mass transfer Stanton number on the suction surface between cases of two different displacement thicknesses

CONCLUSIONS

Mass transfer distributions over the suction surface on a simulated turbine blade have been measured. In the two-dimensional flow region, the mass transfer rate is high in both the leading edge and the trailing edge regions. Along the suction surface, a steep rise following a sharp decrease of the mass transfer distribution indicates that the boundary layer undergoes a laminar separation, transition, and reattachment due to an adverse pressure gradient. The onset of the two-dimensional separation at $S_S/C \approx 1.1$ is insensitive to a change of the exit Reynolds number from 122,000 to 171,000.

In the three-dimensional flow region near the endwall, extremely high mass transfer occurs on the suction surface. This results from the existence of intense corner vortices, the leading edge corner vortex and the suction side corner vortices. The inception point of a particular vortex of the secondary flows can be inferred from the peak of either the spanwise variation or the curvilinear variation in the mass transfer distribution. In addition, the secondary flows inside the blade passage are apparently of sufficient strength to prevent separation of the suction surface boundary layer near the endwall, though separation does occur in the two-dimensional region. Due to the secondary flows and the two-dimensional laminar separation, large variations of the mass transfer occur on the suction surface from a minimum St_m of 0.0005 to a maximum St_m of 0.01.

The spanwise variation of the average mass transfer Stanton number on the suction surface reveals that this average mass transfer rate in the region near the endwall can be several times larger than that in the two-dimensional flow region. An increase of the displacement thickness of the approaching endwall boundary layer from 2.13 mm to 3.18 mm only has a small effect on the mass transfer pattern on the suction surface. Generally speaking, the average mass transfer rate is higher for the case of the thick boundary layer because the region away from the endwall, affected by the secondary flow, is wider for the case of the thick boundary layer.

It should be borne in mind that many particulars of the secondary flows described herein are inferred from the mass transfer distribution. Although these appear quite plausible, confirmation should be sought from direct measurements of the flow in the passage of the cascade including further flow visualization.

ACKNOWLEDGEMENT

Support for this work was provided by the U.S. Air Force Office of Scientific Research. The insightful comments of the reviewers were helpful in improving the final manuscript.

REFERENCES

Abu - Ghannam, B.J., and Shaw, R., 1980, "Natural Transition of Boundary Layers -- The Effects of Turbulence, Pressure Gradient, and Flow History," *J of Mech. Engr. Sci.,* Vol. 22, No. 5, pp. 213 - 228.

Ambrose, D., Lawrenson, I.J., and Sprake, C.H.S., 1975, "The Vapour Pressure of Naphthalene," *J. Chem. Thermodynamics*, Vol. 7, pp. 1173 - 1176.

Arts, T., and Graham C.G., 1985, "External Heat Transfer Study on a HP Turbine Rotor Blade," AGARD-CP-390, *Heat Transfer and Cooling in Gas Turbines,* pp. 5 - 1 to 5 - 6.

Bario, F., Leboeuf, F., and Papailiou, K.D., 1982 "Study of Secondary Flows in Blade Cascades of Turbomachines," ASME *J. of Eng. for Power* , Vol. 104, pp. 497 - 509.

Bayley, F.J., and Priddy, W.J., 1981, "Effects of Free-Stream Turbulence Intensity and Frequency on Heat Transfer to Turbine Blading," ASME *J. of Eng. for Power* , Vol. 103, pp. 60 - 64.

Blair, M.F., 1974, "An Experiment Study of Endwall and Airfoil Surface Heat Transfer in a Large Scale Turbine Blade Cascade," ASME *J. of Heat Transfer,* Vol. 96, pp. 524-529.

Caldwell, L., 1984, "Diffusion Coefficient of Naphthalene in Air and Hydrogen,"*J. Chem. Eng. Data*, Vol. 29, pp. 60 - 62.

Chen, P.H., 1988, "Measurement of Local Mass Transfer from a Gas Turbine Blade," Ph.D. Dissertation, U. of Minnesota, Minneapolis, U.S.A..

Chen, P.H., and Goldstein, R.J., 1988, "Convective Transport Phenomena on a Turbine Blade," Proceedings of the 3rd International Symposium on Transport Phenomena in Thermal Control, Taipei; (1989)*Transport Phenomena in Thermal Control* (edited by G.-J. Hwang), Hemisphere Publishing Corporation, New York, pp. 267-293.

Chen, N.H., and Othmer, D.F., 1962, "New Generalized Equation for Gas Diffusion Coefficient," *J. Chem. Eng. Data*, Vol. 7, No. 1, pp. 37 - 41.

Consigny, H., and Richards, B.E.,1982, "Short Duration Measurements of Heat Transfer Rate to a Gas Turbine Rotor Blade," ASME *J. of Eng. for Gas Turbine and Power*, Vol. 104, pp. 542 - 551.

Daniel, L.D., and Browne, W.B., 1981, "Calculation of Heat Transfer Rates to Gas Turbine Blades," *Int. J. of Heat and Mass Transfer*, Vol. 24, No. 5, pp. 871 - 879.

De Kruif, C.G., Kuipers, T., Van Miltenburg, J.C., Schaake, R.C.F., and Stevens, G., 1981, "The Vapour Pressure of Solid and Liquid Naphthalene," *J. Chem. Thermodynamics,* 13, pp. 1081 - 1086.

Dunn, M.G., and Hause, A., 1982, "Measurement of Heat Flux and Pressure in a Turbine Stage," ASME *J. of Eng. for Power,* Vol. 104, pp. 215 - 223.

Dunn, M.G., Rae, W.J., and Holt, J.L., 1984a, "Measurement and Analyses of Heat Flux Data in a Turbine Stage: Part I - Description of Experimental Apparatus and Data Analysis" ASME *J. of Eng. for Gas Turbine and Power,* Vol. 106, pp. 229 - 233.

Dunn, M.G., Rae, W.J., and Holt, J.L., 1984b, "Measurement and Analyses of Heat Flux Data in a Turbine Stage: Part I - Discussion of Results and Comparisons With Predictions" ASME *J. of Eng. for Gas Turbine and Power,* Vol. 106, pp. 234 - 240.

Dunn, M.G., and Stoddard, F.J., 1979, "Measurement of Heat-Transfer Rate to a Gas Turbine Stator," ASME *J. of Eng. for Power,* Vol. 101, pp. 275.

Dyban, Ye.P., 1982, "Heat Transfer in High-Temperature Gas Turbine," *HEAT TRANSFER - Soviet Research*, Vol. 14, No. 4, pp. 90 - 106.

Dyban, Ye.P., and Glushchenko, V.G, 1975, "Effect of the Mach Number Temperature Factor on Heat Transfer from a Gas to a Turbine Blade," *HEAT TRANSFER - Soviet Research*, Vol. 7, No. 2, pp. 17 - 21.

Eckert, E.R.G., 1976, "Analogies to heat transfer processes," *Measurement in Heat Transfer,* (ed. Eckert, E.R.G., and Goldstein, R.J.), Hemisphere Publishing, New York.

Fowler, C.E., Trump, W.N., and Vogler, C.E., 1968,"Vapor Pressure of Naphthalene : New Measurements between 40° and 180°C," *J. Chem. Eng. Data,* Vol. 13, No. 2, pp. 209 - 210.

Goldstein, R.J., and Chen, P.H., 1987, "Film Cooling on a Turbine Blade with Injection Through Two Rows of Holes in the Near-End-Wall Region," ASME*J. of Turbomachinery*, Vol. 109, pp. 588 - 593.

Goldstein, R.J., and Karni, J., 1984, "The Effect of a Wall Boundary Layer on Local Mass Transfer From a Cylinder in Crossflow," *J. of Heat Transfer*, Vol. 106, pp. 260-267.

Goldstein, R.J., and Spores, R.A., 1988, "Turbulent Transport on the Endwall in the Region Between Adjacent Turbine Blades," ASME *J. of Heat Transfer*, Vol. 110, pp. 862-869.

Graziani, R.A., Blair, M.F., Taylor, J.R., and Mayle, R.E., 1980, "An Experimental Study of Endwall and Airfoil Surface Heat Transfer in a Large Scale Turbine Blade Cascade," ASME *J. of Eng. for Power,* Vol. 102, pp. 257 - 267.

Guenette, G.R., Epstein, A.H., Giles, M.B., Haimes, R., and Norton, R.J.G., 1989, "Fully Scaled Transonic Turbine Rotor Heat Transfer Measurements," ASME *J. of Turbomachinery*, Vol. 111, pp. 1 - 7.

Hippensteele, S.A., Russell, L.M., and Torres, F.J., 1985, "Local Heat-Transfer Measurements on a Large Scale-Model Turbine Blade Airfoil Using a Composite of a Heater Element and Liquid Crystal," ASME Paper No. 85-GT-59.

Hippensteele, S.A., Russell, L.M., and Torres, F.J., 1987, "Use of a Liquid-Crystal, Heater-Element Composite for Quantitative, High-Resolution Heat Transfer Coefficients on a Turbine Airfoil, Including Turbulence and Surface Roughness Effects," NASA-TM-87355, Washington.

Hodson, H.P., and Dominy, R.G., 1987a, "Three-Dimensional Flow in a Low-Pressure Turbine Cascade at Its Design Condition," ASME *J. of Turbomachinery*, Vol. 109, pp. 201 - 209.

Hodson, H.P., and Dominy, R.G., 1987b, "The Off-Design Performance of a Low-Pressure Turbine Cascade," ASME *J. of Turbomachinery*, Vol. 109, pp. 201 -209.

Hoheisel, H., Kiock, R., Lichtfuss, H.J., and Fottner, L., 1987, "Influence of Free-Stream Turbulence and Blade Pressure Gradient on Boundary Layer and Loss Behavior of Turbine Cascades," ASME *J. of Turbomachinery*, Vol. 109, pp. 210 - 219.

Ito, S., Goldstein, R.J., and Eckert, E.R.G., 1978, "Film Cooling of a Gas Turbine Blade." ASME *J. of Eng. for Power,* Vol. 100, pp. 476 - 480.

Kan, S., Miwa, K., Morishita, T., Munakata, Y., and Nomura, M., 1971, "Heat Transfer of a Turbine Blade," *Tokyo Joint Int. Gas Turbine Conference and Products Show*, JSME-30.

Kestin, J., and Wood, R.T., 1971, "The Influence of Turbulence on Mass Transfer from Cylinders," ASME *J. of Heat Transfer*, pp. 321 - 327.

Kline, S.J., and McClintock, F.A., 1953, "Describing Uncertainty in Single-Sample Experiments," *Mechanical Eng.*, Vol. 75, pp. 3 - 8.

Lowery, G.W., and Vachon, R.I., 1975, "The Effect of Turbulence on Heat Transfer from Heated Cylinder," *Int. J. Heat Mass Transfer*, Vol. 18, pp. 1229-1242.

Mack, E., Jr., 1925, "Average Cross-Section Areas of Molecules by Gaseous Diffusion Methods," *J. Am. Chem. Soc.,* Vol. 47, pp. 2468.

Martin, B.W., Brown, A., and Garrett, S.E., 1978, "Heat Transfer to a PVD Rotor Blade at High Subsonic Passage Throat Mach Numbers," *Proc. Inst. Mech. Engr.*, Vol. 192, pp. 225 - 233.

Mukherjee, D.K., 1979, "Determination of Heat Transfer Coefficients Around a Blade Surface from Temperature Measurements," ASME Paper No. 79-GT-28.

Nealy, D.A., Mihelc, M.S., Hylton, L.D., Gladden, H.J., 1984, "Measurements of Heat Transfer Distribution Over the Surfaces of Highly Loaded Turbine Nozzle Guide Vanes," ASME *J. of Eng. for Gas Turbine and Power,* Vol. 106, pp. 149 - 158.

Nicholson, J.H., Forest, A.E., Oldfield, M.L.G., and Schultz, D.L., 1982, "Heat Transfer Optimized Turbine Rotor Blades-An Experimental Study Using Transient Techniques," ASME Paper No. 82-GT-304.

Ota, T., Aiba, S., Tsuruta, T., and Kaga, M., 1983, "Forced Convection Heat Transfer from an Elliptic Cylinder of Axis Ratio 1:2," *Bull. of the JSME*, Vol. 26, No. 212, pp. 262 - 267.

Priddy, W.J., and Bayley, F.J., 1985, "Effects of Free-stream Turbulence on the Distribution of Heat Transfer around Turbine Blade Sections," *Int. J. Heat and Fluid Flow*, Vol. 6, No. 3, pp. 181 - 192.

Sato, T., and Takeishi, K., 1987, "Investigation of the Heat Transfer in High Temperature Gas Turbine Vanes," ASME Paper No. 87-GT-137.

Sato, T., Aoki, S.,Takeishi, K. and Matsuura, M., 1987, "Effect of Three-Dimensional Flow Field on Heat Transfer Problems of a Low Aspect Ratio Turbine Nozzle," 1987 Tokyo International Gas Turbine Congress, 87 -TOKYO - IGTC - 59.

Sharma, O.P., and Bulter, T.L., 1987, "Predictions of Endwall Losses and Secondary Flows in Axial Flow Turbine Cascades," ASME *J. of Turbomachinery*, Vol. 109, pp. 229 - 236.

Sieverding, C.H., and Van Den Bosche, P., 1983, "The Use of Coloured Smoke to Visualize Secondary Flows in a Turbine-Blade Cascade," *J. of Fluid Mech.*, Vol. 134, pp. 85 - 89.

Sieverding, C.H., 1985, "Recent Progress in the Understanding of Basic Aspects of Secondary Flows in Turbine Blade Passages," ASME *J. of Eng. for Gas Turbine and Power*, Vol. 107, pp. 248 - 257.

Smith, A.G., 1948, "Heat Flow in the Gas Turbine," *Proc. Inst. Mech. Engr.*, Vol. 159, pp. 245 - 254.

Sonoda, T., 1985, "Experimental Investigation on Spatial Development of Streamwise Vortices in a Turbine Inlet Guide Vane Cascade," ASME Paper No. 85-GT-20.

Taylor, J.R., 1980, "Heat Transfer Phenomena in Gas Turbines," ASME Paper No. 80-GT-172.

Turner, A.B., 1971, "Local Heat Transfer Measurements on a Gas Turbine Blade," *J. Mech. Eng. Sci.,* Vol. 103, No. 1, pp. 1 - 12.

Turner, A.B., Tarada, F.H.A., and Bayley, F.J., 1985, "Effect of Surface Roughness on Heat Transfer to Gas Turbine Blades," AGARD-CP-390, *Heat Transfer and Cooling in Gas Turbines*, pp. 9 - 1 to 9 - 10.

Van Ekeren, P.J., Jacobs, M.H.G., Offringa, J.C.A., and De Kruif, C.G., 1983, "Vapor-Pressure Measurements on Trans-diphenylethene and Naphthalene Using a Spinning-rotor Friction Gauge," *J. Chem. Thermodynamics,*, Vol. 15, pp. 409 - 417.

Walker, L.A., and Markland, E., 1965, "Heat Transfer to Turbine Blading in the Presence of Secondary Flow," *Int. J. of Heat and Mass Transfer*, Vol. 8, pp. 729 - 748.

Wang, J.H., Jen, H.F., and Hartel, E.O., 1985, "Airfoil Heat Transfer Calculation Using a Low Reynolds Number Version of a Two-Equation Turbulence Model," ASME *J. of Eng. for Gas Turbine and Power*, Vol. 107, pp. 60 - 67.

Wilson, D.G., and Pope, J.A., 1954, "Convective Heat Transfer to Gas Turbine Blade Surfaces," *Proc. Inst. Mech. Engr.*, Vol. 168, pp. 861 - 874.

Winstanley, D.K., Booth, T.C., and Dunn, M.G., 1981, "The Predictability of Turbine Vane Convection Heat Transfer," AIAA Paper No. AIAA-81-1435.

Yamamoto, A., 1987, "Production and Development of Secondary Flows and Losses in Two Types of Straight Turbine Cascades: Part 1- A Stator Case," ASME *J. of Turbomachinery*, Vol. 109, pp. 186 - 200.

Yamamoto, A., and Nouse, H., 1988, "Effects of Incidence on Three-Dimensional Flows in a Linear Turbine Cascade," ASME *J. of Turbomachinery*, Vol. 110, pp. 486 - 496.

York, R.E., Hylton, L.D., Fox, R.G., Jr., and Simonich, J.C., 1979, "An Experimental Investigation of the Heat Transfer to a Turbine Vane at Simulated Engine Conditions," ASME Paper No. 79-GT-23.